Brian P. Trease
Doctoral Pre-candidate
e-mail: trease@asme.org
Department of Mechanical Engineering,
The University of Michigan,
Ann Arbor, MI 48109
Phone: 734.763.4916

Yong-Mo Moon
Assistant Professor
e-mail: moon@wpi.edu
Department of Mechanical Engineering,
Worcester Polytechnic Institute,
Worcester, MA 01609

Sridhar Kota
Professor
e-mail: kota@umich.edu
Department of Mechanical Engineering,
The University of Michigan,
Ann Arbor, MI 48109

Design of Large-Displacement Compliant Joints

This paper investigates the drawbacks of typical flexure connectors and presents several new designs for highly effective, kinematically well-behaved compliant joints. A revolute and a translational compliant joint are proposed, both of which offer great improvements over existing flexures in the qualities of (1) a large range of motion, (2) minimal "axis drift," (3) increased off-axis stiffness, and (4) a reduced stress-concentrations. Analytic stiffness equations are developed for each joint and parametric computer models are used to verify their superior stiffness properties. A catalog of design charts based on the parametric models is also presented, allowing for rapid sizing of the joints for custom performance. A joint range of motion has been calculated with finite element analysis, including stress concentration effects. [DOI: 10.1115/1.1900149]

Introduction

Rigid mechanical connections, such as hinges, sliders, universal joints, and ball-and-socket joints, allow different kinematic degrees of freedom between connected parts. However, the clearance between mating parts of rigid joints causes backlash in mechanical assemblies. Further, in all of the above joints there is relative motion causing friction that leads to wear and increased clearances. A kinematic chain of such joints compounds the individual errors from backlash and wear, resulting in poor accuracy and repeatability. The prospect for improvement in these last two qualities is a key impetus for the research of new joints.

The objective of this research is to provide a flexible means of connecting parts using large-displacement compliant joints (see Fig. 1). Flexible joints (a.k.a. flexures) utilize the inherent compliance of a material rather than restrain such deformation. These joints eliminate the presence of friction, backlash, and wear. Further benefits include up to sub-micron accuracy due to their continuous monolithic construction. Such accuracy is important in many micro-, nano-, and bio-applications. The monolithic construction also simplifies production, enabling low-cost fabrication.

In the last 50 years, many flexible joints have been researched and developed, most of which are considered one of two varieties: Notch-type joints [Figs. 2(*a*) and 2(*b*)] [also see Tables 1(*b*)–(*d*) and 2(*a*)] and leaf springs [Fig. 2(*c*)] [also see Tables 1(*a*) and 2(*b*)–(*i*)]. Notch-type flexible joints (a.k.a. fillet joints) were first analyzed by Paros and Weisbord in 1965 [1] and have since become well understood by many researchers and designers. Today, notch-type joint assemblies are widely used for high-precision, small-displacement mechanisms [2]. These joints have also been applied by Howell and Midha [3] to develop the field of pseudo-rigid-body compliant mechanisms. See Lobontiu for the most current analyses of planar [4] and spherical three-dimensional (3D) [5] *filleted* notch joints. For the inverse static analysis of a planar system with flexural pivots, please see Carricato et al. [6].

Leaf springs provide the most generic flexible translational joint, composed of sets of parallel flexible beams [Fig. 2(*c*)]. In addition to high-precision motion stages, leaf spring joints are also widely used in medical instrumentation [7] and MEMS devices [8].

Contributed by the Mechanical Design Division for publication in the JOURNAL OF MECHANICAL DESIGN. Manuscript received March 6, 2004. Final manuscript received November 7, 2004. Review conducted by: G. K. Ananthasuresh.

The benefits gained from using conventional flexure joints come at the cost of several disadvantages that must be taken into account when designing. To overcome these drawbacks and develop better flexures, a set of criterion must be established for benchmarking. The four most important criterion are (1) the range of motion, (2) the amount of axis drift, (3) the ratio of off-axis stiffness to axial stiffness, and (4) stress concentration effects.

Range of Motion. All flexures are limited to a finite range of motion, while their rigid counterparts rotate infinitely or translate long distances. The range of motion of a flexible joint is limited by the permissible stresses and strains in the material. When the yield stress is reached, elastic deformation becomes plastic, after which, joint behavior is unstable and unpredictable. Therefore, the range of motion is determined by both the material and geometry of the joint.

Axis Drift. In addition to a limited range of motion, most flexure joints also undergo imprecise motion referred to as axis drift or parasitic motion. For notch-type joints, the center of rotation does not remain fixed with respect to the links it connects. With translational flexures, there can be considerable deviation from the axis of straight-line motion. For example, a simple four-bar leaf spring experiences curvilinear motion.

The axis drift can be improved by adding symmetry to the design of a joint. However, this often increases the stiffness of the joint in the desired direction of motion. Further, more space is required to accommodate any symmetric joint components.

Off-Axis Stiffness. While most flexure joints deliver some degree of compliance in the desired direction, they typically suffer

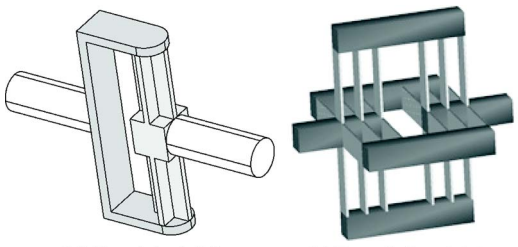

(a) Revolute Joint **(b)** Translational Joint

Fig. 1 Proposed compliant joints

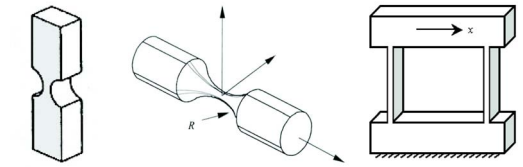

Fig. 2 Basic flexible joint components

from low rotational and translational stiffness in other directions. A high ratio of off-axis to axial stiffness is considered a key characteristic of an effective compliant joint.

Stress Concentration. Most notch-type joints have areas of reduced cross section through which their primary deflection occurs. Depending on the shape of these reduced cross sections, the joints may be prone to high stress concentrations and hence a poor fatigue life. Refer again to Figs. 2(*a*) and 2(*b*) for examples of flexures with stress concentrations.

Related Research

As mentioned, primitive joints previously developed typically fall into one of two categories: Notch joints or leaf spring joints.

Table 1 Benchmarked flexible translational joints (–: poor, 0: normal; +: good)

		Range of Motion	Axis Drift	Stress Concentration	Off-Axis Stiffness	Compactness
(a)	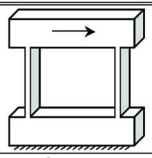	0	–	0	0	+
(b)	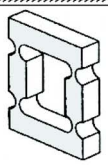	–	–	–	0	+
(c)	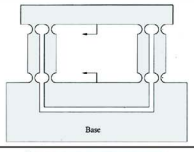	–	0	–	0	+
(d)	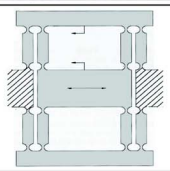	–	+	–	0	+
(e)	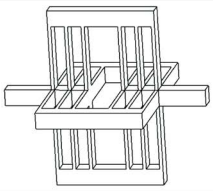	+	+	+	+	+

These joints are often combined in assemblies and are most commonly used as revolute joints, universal joints, or parallel four-bar translational joints. Most commercially available flexible joints are such derivatives of the primitive joints, with the addition of any variety of packaging and connections to suit particular engi-

Table 2 Benchmarked flexible revolute joints

		Range of Motion	Axis Drift	Stress Concentration	Off-Axis Stiffness	Compactness
(a)	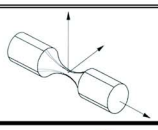	–	–	–	–	+
(b)	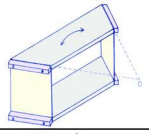	0	–	+	–	0
(c)	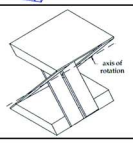	+	–	+	–	–
(d)		–	–	0	–	+
(e)	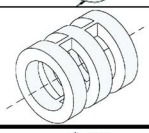	–	0	–	0	0
(f)	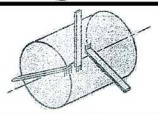	–	+	0	–	–
(g)	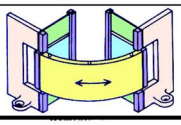	+	+	+	–	–
(h)	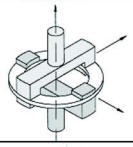	–	+	–	–	–
(i)		–	0	–	–	0
(j)	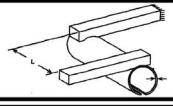	+	0	+	+	0
(k)	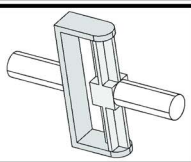	+	+	+	+	0

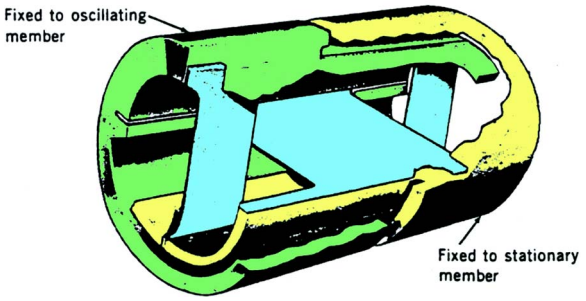

Fig. 3 Commercial "free-flex" or "cross-spring" joint

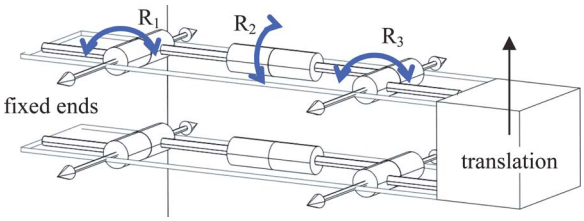

Fig. 4 One DOF configuration for translation

neering needs. For a detailed study of traditional flexures, including design methods, material selection, and geometry optimization, please refer to Lobontiu [9].

Most of the existing translational joints are based on a parallel four-bar building block. Their flexibility is derived from leaf springs [Table 1(*a*)] or notch joints [Table 1(*b*)]. The compound four-bar joints in Tables 1(*c*) and 1(*d*) deliver a larger range of straight-line motion. All four joints have acceptable off-axis stiffness, but the range of motion is very limited, even for the compound joints. The newly proposed compliant translational joint is shown in Table 1(*e*). While the *spatial*, 3D version of the CT joint is shown, it and the other translational joints are ranked "good" for compactness based on their *planar* versions.

The comparisons offered in this paper are primarily qualitative rather than quantitative. The purpose is to characterize the existing joints based on their inherent form without respect to scale. For example, the range of motion of many flexures can be doubled by simply doubling the size. A comparison that provides actual numbers would require some normalization (e.g., equivalent device footprints or characteristic lengths) and is an interest to be considered in future research.

Many revolute joints have also been created using notch and leaf spring primitives. Table 2(*a*) shows a spherical joint created by a cylindrical notch cut. Refer to Lobontiu [5] for analysis of such spherical joints. Leaf springs can also be used in a variety of ways to create revolute joints, as shown in Tables 2(*b*) [10], 2(*c*) [11], 2(*d*) [7], and 2(*e*) [7]. Table 2(*c*) is also recognized as the well-known "free-flex" or "cross-spring" pivot, commercially available in many forms (see Fig. 3).

Two leaf spring joints that offer almost no axis drift are depicted in Tables 2(*f*) [12] and 2(*g*) [10]. However, the triple-leaf spring [Table 2(*f*)] offers a limited range of motion and both joints are bulky and have only moderate off-axis stiffness.

Universal joints fabricated from *circular* leaf springs are shown in Tables 2(*h*) and 2(*i*) [7]. Both of these joints also provide axial translation, which is useful in self-alignment applications. However, they both have stress concentrations which limits their range of motion.

Goldfarb et al. [13] suggest a split-tube revolute joint, shown in Table 2(*j*). This joint offers the off-axis stiffness of a solid circular tube while having a low torsional stiffness. While the axis drift of a split-tube is small, it is not zero. Perfect rigidity would require infinitely thin line contact between the connecting link and the tube. Further, this joint exhibits a tradeoff between range of motion and off-axis stiffness. Under large displacements, the gap separation increases and the tube warps out of circular shape, reducing the off-axis stiffness.

Our proposed compliant revolute joint, shown in Table 2(*k*), maintains zero axis drift under moment-loading. Of all the flexible revolute joints, it is the only one to have a large range of motion combined with a high ratio of off-axis stiffness to stiffness in the desired direction of motion. In comparison, the rotation axis of a popular cross-spring pivot [Fig. 2(*c*)] of comparable size to our joint (diagonal leaf-springs 114 mm long) drifts 5.5 mm while rotating through 40 deg. (See Haringx [14] for design tables.) Even under typical axial loading, the proposed compliant joint's axis of rotation drifts only nanometers, as described later in this paper.

It is part of our continuing research to improve the manufacturability of the CR joint. With the use of cruciform cross-section extrusions, we intend for the fabrication of the joint from parts found in local hardware stores.

Compliant Translational Joint

Conceptual Design. The compliant translational (CT) joint, shown in Fig. 5, is proposed as a novel improvement of the leaf spring joint. The problems typical leaf spring joints encounter are poor off-axis stiffness, limited range of motion, and deviation from straight-line motion.

A plate can be modeled as a serial kinematic chain with three rotational degrees of freedom (DOF), as depicted in Fig. 4. The rotation DOF (R_2) along the plate is constrained by the parallel arrangement of two identical plates that from an equivalent four-bar linkage system. The parallel four-bar mechanism allows only pure translational motion on a curvilinear trajectory. With a symmetric arrangement of the parallel four-bar linkage systems as in Fig. 5(*a*), pure translational motion without axis drift is possible, resulting in our CT joint concept.

The off-axis (lateral) stiffness of the planar joint is due to the axial stiffness of the individual beams and is, therefore, proportional to beam cross-section area, A. Beam bending provides the axial (translational) stiffness which is, therefore, proportional to the area moment of inertia, I_B. Increasing the ratio of the off-axis stiffness to the axial stiffness requires increasing the area while decreasing I_B. This is accomplished in the CT joint by using groups of three parallel leaf springs rather than two. The formulas for the simple two and three beam cases are derived in Table 3. The last row of the table shows that by simply increasing the number of beams while keeping the total area constant, the stiffness ratio is increased by $9/4=2.25$.

Using *distributed* compliance in long beams, rather than *lumped* compliance in short and narrow cross sections, allows for greater displacements before local joint yielding. Having *multiple* thin beams further increases the range of motion, but at the cost of

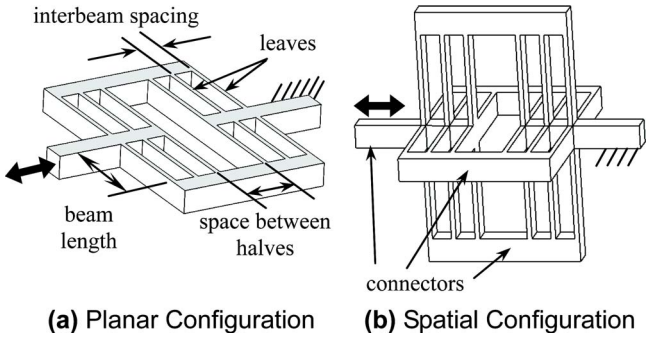

Fig. 5 CT joint conceptual designs

Table 3 Stiffness ratios for multiple beam flexures

(both figures have the same out-of-plane beam width)

off-axis / axis	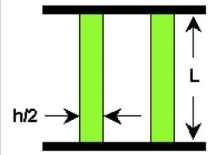	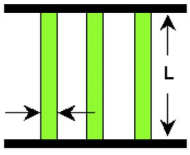
Off-Axis Stiffness	$\frac{EA}{L}=\frac{Ewh}{L}$	$\frac{EA}{L}=\frac{Ewh}{L}$
Axial Stiffness	$2\cdot\left(12\frac{EI_B}{L^3}\right)=3\frac{Ewh^3}{L^3}$	$3\cdot\left(12\frac{EI_B}{L^3}\right)=\frac{4}{3}\frac{Ewh^3}{L^3}$
Stiffness Ratio*	$\frac{1}{3}\left(\frac{L}{h}\right)^2$	$\frac{3}{4}\left(\frac{L}{h}\right)^2$

*Stiffness Ratio = Off-Axis Stiffness / Axial Stiffness

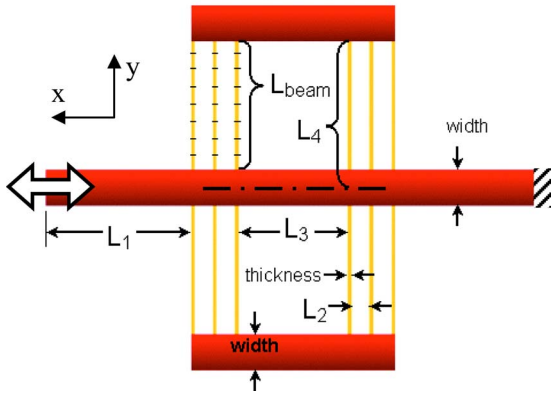

Fig. 6 CT joint parameters used in ADAMS model

the maximum load carried. The load is distributed among all the beams, and thin beams can flex farther than thick beams before the maximum bending stress is reached. Linear analysis indicates a 50% increase in the range of motion with a 33% reduction in load-carrying capability.

When off-axis forces are applied outside of the group of beams, the three-beam construction offers the benefit of reduced compressive loads. With only two beams under such loading, both are in compression. For three beams, however, the center beam acts as a pivot, putting one beam in compression and the beam farthest from the applied load in tension. With both tension and compression present, the compressive loads are actually reduced, allowing for a greater safety factor against buckling.

Straight-line motion is achieved by the symmetry of the configuration. The planar CT joint has two sets of leaf springs symmetric about the longitudinal axis. The spatial configuration is two planar CT joints intersecting at 90 deg, giving it rotational symmetry about its axis of motion.

Analytical Modeling of Compliant Translational Joint. The flexibility of the CT joint comes from simple cantilever elements (leaves) of rectangular cross section. The remaining elements (connectors) are considered rigid. While the displacements being analyzed are large compared to notch-type joints, they are still relatively small when considered as cantilevers and remain in the realm of linear theory. Calculating the axial translational stiffness is straightforward; the structure of the *planar* CT joint is 2 sets of 6 parallel cantilever beams, connected in series. The resulting axial stiffness is 3 times that of a single beam.

$$k_{\text{axial(planar)}}=3\frac{Et^3w}{L_B^3} \tag{1}$$

With respect to axial stiffness, the spatial joint is essentially two planar joints working in parallel, giving the spatial joint twice the stiffness of the planar joint:

$$k_{\text{axial(spatial)}}=6\frac{Et^3w}{L_B^3} \tag{2}$$

The remaining off-axis stiffnesses are provided by numerical software analysis in the next section.

Parametric Numerical Model of Compliant Translational Joint. MSC's ADAMS software was used for motion analysis of both the CR and CT joints. Fully parametric, three-dimensional, flexible models were created to be quickly reconfigured to any design specification. The discrete flexible links used in ADAMS can deflect under axial, bending, shear, and torsional loads. The connecting members are still considered rigid. For all of the CT results given in this report, the flexible members have been designated as aluminum with $E=73$ GPa and $G=27$ GPa. The ADAMS model of the CT joint (Fig. 6) consists of 24 flexible beams connected by 6 rigid connectors. Each flexible beam is divided into 8 flexible elements.

For clarity, the stiffness values of a typical CT joint are listed in Table 4. The dimensions used are: Width $(w)=10$ mm, $t=1$ mm, $L_1=40$, $L_2=5$ mm, $L_3=24$ mm, and $L_B=30$ mm. Off-axis motion is described by the lateral rotational stiffness $(M_y/\theta_y, M_z/\theta_z)$ and the axial rotational stiffness (M_x/θ_x). The axial stiffness exactly matches that predicted by Eq. (2).

To truly appreciate the stiffness ratios, they must be divided by the moment arm squared, achieving a unitless ratio. The moment arm in this case is half the joint's total x length. In our case (moment arm=65 mm), the two ratios become 2.85 and 2.28, respectively. In other words, the CT joint is 2.85 times stiffer in an off-axis direction for lateral forces applied at the tip.

CT Joint Range Of Motion. Since axial motion requires only simple beam-bending, a single linear formula, Eq. (3), is sufficient to determine the CT range of motion, as limited by the material yield stress. With the series arrangement of the beams, the CT range of motion (x_t) is twice that of a single beam (x_b). These formulas work for both planar and spatial joints.

$$x_b=\frac{1}{3}\frac{L^2}{t}\frac{\sigma_y}{E};\quad x_t=2x_b=\frac{2}{3}\frac{L^2}{t}\frac{\sigma_y}{E} \tag{3}$$

Note that the range of motion is a function of only three parameters: L, t, and material (σ_y/E). For a given material, such as aluminum $(\sigma_y/E=414/73100=0.0057)$, the ROM is depicted in Fig. 7. For comparative (σ_y/E) ratios in other materials, see Howell [3], p. 30.

The corresponding load at yield (i.e., the maximum axial load the joint will bear) is found with Eq. (4). The maximum load is independent of E and may be interpreted as a function of only three parameters: Cross-section area $(w\times t)$, material (σ_y), and (t/L). The last quantity can be thought of as a "bending slenderness ratio."

Table 4 Stiffness for sample spatial CT joint

Stiffness	Value from ADAMS	Ratio to k_{axial}
axial (F_x/d_x)	162 N/mm	1
Rotational $(M_y/\theta_y), (M_z/\theta_z)$	1,951,000 N-mm/rad	12,050 mm^2/rad
Rotational (M_x/θ_x)	1,563,749 N-mm/rad	9,650 mm^2/rad

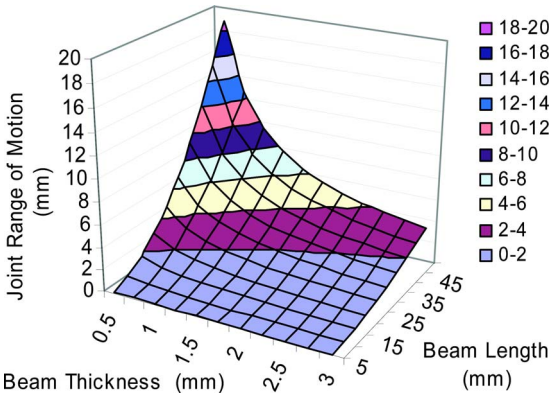

Fig. 7 Parametric range of motion for aluminum CT joint

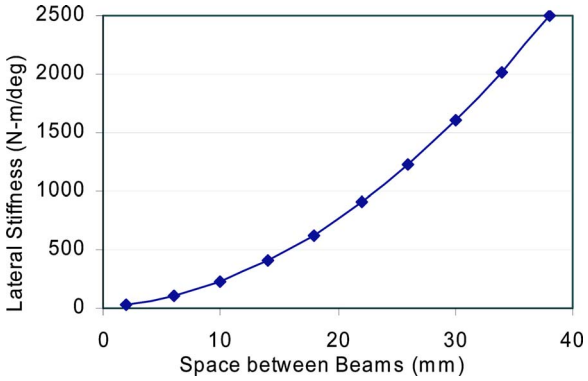

Fig. 9 Lateral stiffness of CT joint (thickness=2 mm, width =10 mm)

$$F_{\max(\text{spatial})} = 12\frac{wt^2}{3L}\sigma_y; \quad F_{\max(\text{planar})} = 6\frac{wt^2}{3L}\sigma_y \tag{4}$$

The range of motion for the joint analyzed in Table 4 (w =10 mm, t=1 mm, L_B=30 mm) is ±3 mm and ±5 mm when made of aluminum and titanium, respectively. A more flexible design is achieved by varying the geometry (w=10 mm, t =0.8 mm, L_B=35 mm) and using plastic (ABS; E=2480 MPa, σ_y=34.5 MPa). The resulting stiffness, range of motion, and maximum load are 1.8 N/mm, ±11.4 mm (depicted in Fig. 8), and 39 N.

Parametric Study. The catalog of graphs obtained from the parametric studies serves as a quick and effective design tool for sizing new joints. If a maximum axial stiffness (F_x/d_x) or minimum lateral stiffness (M_z/θ_z or M_y/θ_y) is specified, that value can be found on the vertical axis of the corresponding graph. For example, when attempting to meet a given axial stiffness, the given value corresponds to a horizontal plane cut through the graph. Many of these planes are already shown in the following figures (e.g., the 200 N m/deg line in Fig. 11). Any point located below this plane indicates the feasible design space left to meet any other design specifications.

A designer may next wish to go to the lateral stiffness graph and find the greatest lateral stiffness that can be achieved from the subspace determined by the previous graph. This technique requires only a few iterations and can be used to meet stiffness requirements, spatial limitations, and weight limitations. The slope of a graph at any point also gives the designer an idea of what changes may be implemented to improve future designs, and by what degree.

The parameters studied include the interbeam spacing (L_2), the length of the input–output arms (L_1), and the beam dimensions (width, thickness, and length). Variations of these parameters were analyzed for their effect on axial and lateral stiffness. Note that ADAMS is used for its parametric stiffness calculations, but is not capable of stress analysis. Therefore, no parametric range-of-motion studies are included.

CT Joint Design Charts. Four studies were performed with the CT joint model, using aluminum material properties. Three of these considered parametric effects on the moment-loaded lateral stiffness (N mm/degree) and are shown in Figs. 9–11. For the designs in Fig. 9, the cross section is held constant: Width =10 mm and thickness=2 mm. It is noted here that the gap between the two halves of the joint (L_3) does not effect the moment-

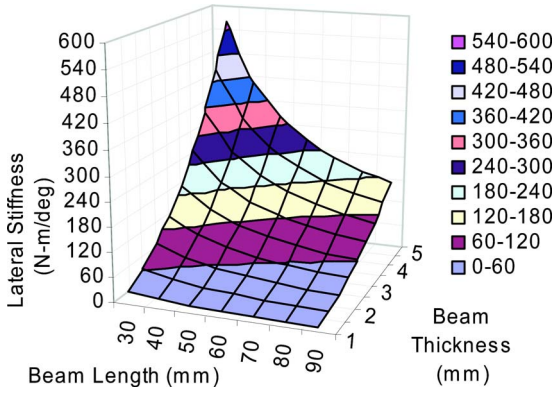

Fig. 10 Lateral stiffness of CT joint (width=10 mm)

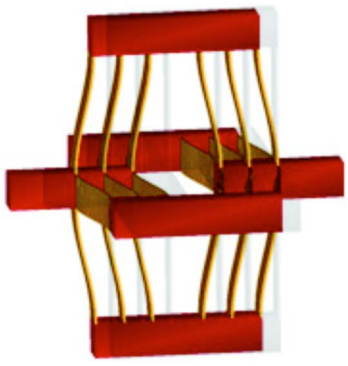

Fig. 8 Range of motion of ABS plastic CT joint

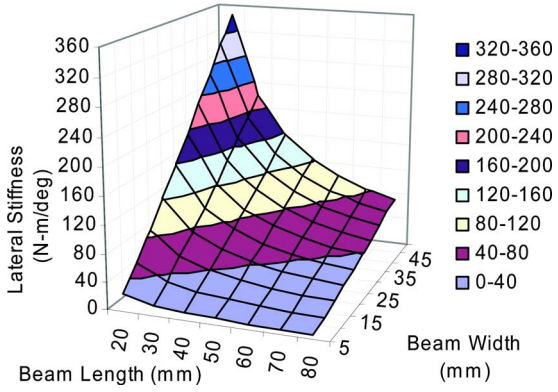

Fig. 11 Lateral stiffness of CT joint (thickness=1 mm)

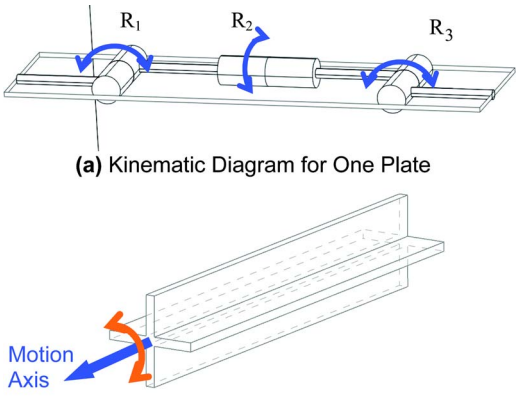

(a) Kinematic Diagram for One Plate

(b) Kinematic Diagram for Two Plates for Rotation

Fig. 12 Kinematic plate configurations

loaded lateral stiffness of the joint.

In Fig. 10, the gap is constant at 30 mm, the interbeam spacing is 5 mm, and the beam width is 10 mm. In Fig. 11, the gap and interbeam spacing are held at the same values, but the beam thickness is instead fixed at 1 mm.

Due to the assumption of rigid connecting members, L_2 and L_3 have no effect on the axial stiffness of the joint. This is evident by visual inspection of the joint. Further, a parametric plot of axial stiffness is unnecessary as a design tool, as Eq. (2) already perfectly describes the relationships. In fact, Eq. (2) can be rewritten as $k_{\text{axial}}=72\ EI_B/L^3$. The analytic equations predict that the axial stiffness should only be a function of I_B, which takes into account both the beam width and thickness. This direct dependence holds only for the axial stiffness; the lateral stiffness has a more complex dependence on beam width and thickness, requiring the two separate studies shown in the previous figures.

Compliant Revolute Joint

Conceptual Design. The compliant revolute (CR) joint is designed to generate pure rotational motion. The majority of the existing flexible revolute joints are notch-type joints with considerable axis drift.

As demonstrated for the CT joint, a simple plate has three degrees of freedom, depicted again in Fig. 12(*a*). For a CR joint, only the torsional DOF (R_2) should be present; the two bending DOF's (R_1 and R_3) should be constrained or reduced. Therefore, two plates are configured as in Fig. 12(*b*) so that the bending DOF's are constrained and the total DOF is one.

Using the configuration in Fig. 12(*b*), the CR joints in Fig. 13 are constructed. The CR joints rely on torsion of the connecting plates to provide very large compliance about their axes and a large range of motion compared to the notch-type revolute joints. The intended axis of motion (rotation in this case) is called the

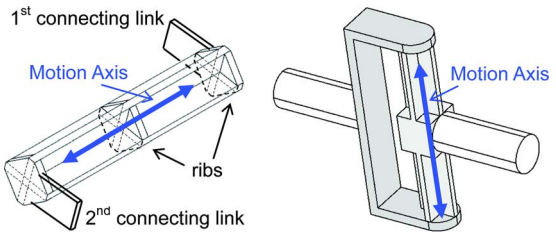

(a) End-Moment CR Joint **(b)** Center-Moment CR Joint

Fig. 13 Cross-type compliant revolute joints

Table 5 Analytic CR joint stiffness formulas

Torsional Stiffness	k_{66} (M_z/θ_z)	$\left(\frac{w}{t}-0.373\right)\frac{4G\,t^4}{3L}$
Bending / Rotational Stiffness	k_{44} (M_x/θ_x), k_{55} (M_y/θ_y)	8 EI/L
Bending Stiffness	k_{11} (F_x/d_x), k_{22} (F_y/d_y)	24 EI/L^3
Axial Stiffness	k_{33} (F_z/d_z)	2 AE/L

Note 1: $I_x = I_y = I = 1/12*(wt^3 + tw^3 - t^4)$; $A = 2wt - t^2$

Note 2: Displacements, d_i, are at the joint center

motion axis or the functional axis. The joint is designed to be very stiff against forces or torque in all other directions (i.e., high off-axis stiffness).

We are presenting two different CR joints: Cross [*a.k.a. End-Moment CR*, see Fig. 13(*a*)] and Segmented-Cross [*a.k.a. Center-Moment CR*, see Fig. 13(*b*)]. Cross-type CR joints have ribs to prevent bending and reduced cross sections to provide torsional compliance. For the segmented joint, the connecting rod acts as a rib. A minimum distance is maintained between the ends of the joint and the rib to provide torsional compliance yet resist bending about the other two orthogonal axes. The range of motion can be adjusted by changing the length of the beams. The remainder of this paper focuses on Center-Moment (Segmented-Cross) joints.

Analytic Stiffness Formulation. Most of the stiffness components of the CR joint, except for the primary rotational stiffness, can be calculated with standard beam formulas. An empirical formula for the rotational stiffness of a cruciform hinge, accurate to within 4%, is described by Smith [7]. A cruciform hinge is a torsion bar with a cross-shaped cross-section, depicted in Fig. 13(*a*). The CR joint is considered as two cruciform hinges used in parallel [Fig. 13(*b*)], thus having twice the axial, bending, and torsional stiffness suggested by Smith, and 8 times the bending–rotational stiffness. Due to symmetry and loading at the center, the resulting 6×6 spatial stiffness matrix is purely diagonal. The six diagonal elements, based on the coordinates of Fig. 15, are given in Table 5. "*w*" and "*t*" represent the width and thickness, as labeled in Fig. 14.

From Table 5 it can be seen that, for a 3D scaling factor of *s*, the torsional and moment stiffnesses scale as s^3, while the linear stiffnesses (F_i/d_i) scale directly proportional to *s*. Thus, smaller joints generally have a very high torsional to off-axis stiffness ratio, except for the rotational off-axis stiffness. The moments M_x and M_y would have to be small for the benefit to be realized.

The stiffness values for a typically-sized, titanium CR joint are calculated and displayed in Table 6 ($E=120$ GPa, $G=44$ GPa). The dimensions used are: Width=10 mm, thickness=0.8 mm, beam length=40 mm. To illustrate the benefits of this joint, the ratio of each off-axis stiffness with respect to the torsional stiffness is also included.

Because translational and rotational stiffness have different units, their ratio has units of radians/mm^2, which indicates depen-

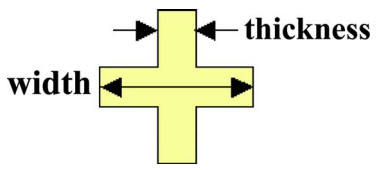

Fig. 14 Cross-section parameters for CR joint

Table 6 Analytic stiffnesses of sample CR joint

Stiffness		Value	Ratio to k_{66}
Torsional	k_{66} (M_z/θ_z)	7,305 N-mm/rad	1
Bending / Rotational	k_{44} (M_x/θ_x), k_{55} (M_y/θ_y)	1,608,600 N-mm/rad	220
Bending	k_{11} (F_x/d_x), k_{22} (F_y/d_y)	3,016 N/mm	1,250
Axial	k_{33} (F_z/d_z)	92,160 N/mm	38,000

Note: Displacements, d_i, are at the joint center

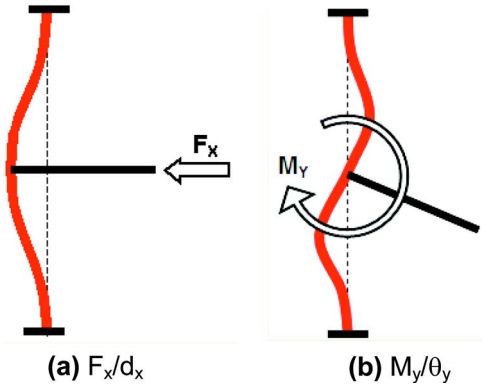

Fig. 16 Graphical depiction of CR joint stiffness

dence on the length of the moment arm (MA). Dimensionless values are attained by multiplying these ratios by MA^2. In Table 6 (MA=55 mm), multiplying the direct ratios (k_{11}/k_{66} =0.413 rad/mm^2 and k_{22}/k_{66}=12.6 rad/mm^2) by (55 mm)^2 gives the modified ratios of k_{11}/k_{66}=1,249 and k_{33}/k_{66}=38,163. With the smallest off-axis ratio at 220 and the others much higher, it is evident that this is a very effective flexible joint.

Finite Element Calculations. Finite element analysis was performed to verify analytic results and evaluate the effect of adding fillets. Fillets are needed to reduce stress-concentrations, as described later in the nonlinear FE range of motion analysis. Two types of end-constraints were also modeled: 1) Rigidly fixed ends, allowing no warping (actual physical case) and (2) point-constrained ends, free to warp (simplified case). Note that the axial center-line length was not allowed to change in either case, as restricted by the actual geometry constraints.

These analyses indicate that the analytic formula derived earlier for rotational stiffness is valid only for the ideal case of no fillets and no warping constraints. (For this case, the value is off by 2%, within the earlier stated 4% accuracy of the formula.) In our trial analyses, the addition of fillets increases the stiffness by 14.4%, and the additional no end-warping constraint increases the stiffness by another 8%, for a total increase of 23.6%. This relative error holds for only this particular geometry; for other typical joints the analytic underestimation ranges from ~25–40%.

Numerical Stiffness Calculations. While range of motion requires large-deformation finite element analysis (see later section), linear numerical motion analysis in ADAMS is sufficient for finding off-axis stiffness values. The ADAMS models are easily made parametric, allowing for creation of multi-parameter design curves. Because of the ease in incorporating rigid body motions, the ADAMS models offer better off-axis stiffness accuracy than the analytic models. The CR joint, shown in Fig. 15, consists of two beams each of 8 flexible elements, connected in the middle by a rigid arm. The desired motion of this joint is rotation about the longitudinal axis of the flexible beams (θ_z). Not only were all

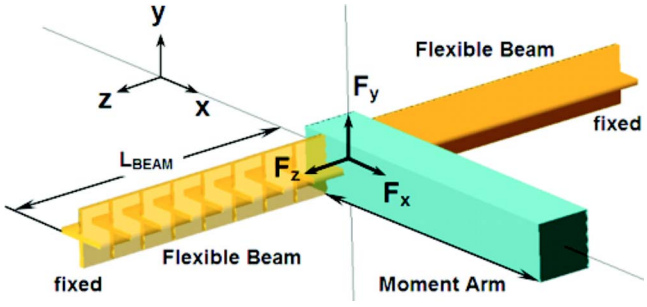

Fig. 15 Computer model of CR joint

stiffnesses of this joint considered, but also the drift of the center of rotation for various loading conditions. A rigid center of rotation, which is not found in most traditional flexible joints, is critical in emulating the kinematics of true revolute joints. The parameters studied in the CR joint include the cross section of the beams, defined by the thickness and width (see Fig. 14), the length of the beams, and the length of the moment arm.

From analysis of the above typical joint, the center of rotation drift (CRD) is determined to be minimal. During normal moment-loaded operation there is *no CRD* for any degree of rotation. If x direction loading is present during operation, it contributes only 331 nm to the CRD per Newton of applied force, F_x. These values indicate negligible drift for practical applications.

The substantial error in the analytic rotational off-axis stiffness (see Table 7) is due to the accounted rigid body motion of the block connecting the two segments. The formula for this stiffness typically underpredicts from 6% to 30%.

CR Joint Stiffness Design Charts. The motivation for parametric studies is the same as described earlier in the CT joint section. Nine dual-parameter studies were done with the titanium CR joint, represented by 3D surface plots of the output variables. The nine studies consisted of three groups to evaluate torsional stiffness (M_z/θ_z), bending stiffness (F_x/d_x) [see Fig. 16(a)], and bending–rotational stiffness (M_y/θ_y) [see Fig. 16(b)]. In each of these studies, the following three combinations of parameters were inspected:

- Width and Length
- Thickness and Length
- Width and Ratio of Thickness to Width (RTW)

Of the nine studies, several significant ones are included in this report. As with the CT joints, these parametric studies serve as design charts to aid in creating new joints. Interested readers may contact the authors to obtain the complete set of design charts.

The first quantity considered reflects the desired motion of the joint: Torsional compliance. To maximize the desired compliance, the torsional stiffness, illustrated in Figs. 17 and 18, must be minimized. The first plot indicates that stiffness decreases nonlinearly with respect to width when the RTW is constant and vice versa.

Figure 18 shows the combined effects of beam length and width on the torsional stiffness. Beam width has only a linear effect on stiffness for a given beam length. However, beam length nonlinearly decreases the stiffness for a given width.

While the first two plots suggest small widths, small thicknesses, and long beams for minimal torsional stiffness, these conflict with the requirements for maximum off-axis stiffness. This requires referring to Fig. 19, which shows the rotational bending stiffness, illustrated in Fig. 16(b). From the plot, it is evident that

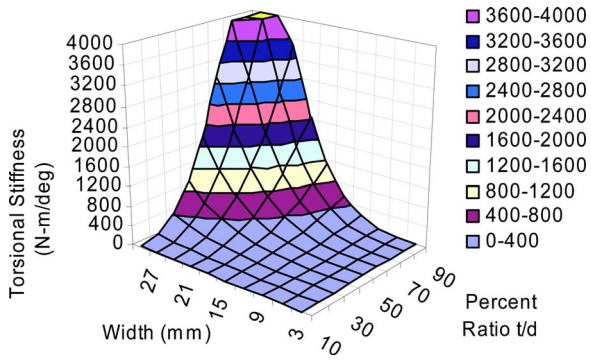

Fig. 17 *z*-rotational stiffness of CR joint (beam length =50 mm)

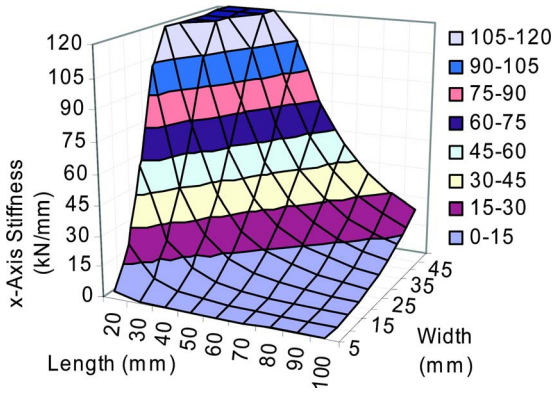

Fig. 20 *x*-bending stiffness of CR joint (thickness=1 mm)

maximum bending stiffness requires shorter beams with thicker flanges. This contradiction verifies the need for a design tool to balance both objectives.

Figure 20 shows the stiffness of the CR joint when it is loaded as a fixed–fixed beam with a perpendicular force (i.e., x direction) applied at its center, as in Fig. 16(a). Increased width and reduced length are required to increase the x axis stiffness. The effect of width is nearly linear for a given length, but the length has a nonlinear effect for a constant width.

Analytic Range of Motion. The range of motion is determined as the amount of deflection which causes yielding in the material. Analytic and finite element solutions are both offered, with comparable results. Linear analytic equations derived for the CR joint are based on several assumptions. Norton [15] provides the torque–stress relationship in Eq. (5).

$$\tau_{\max} = \frac{T}{Q}$$

$$(\textit{for circles},\ Q = J/r; J = \textit{polar moment of intertia}) \qquad (5)$$

Note that $T=k_\theta\theta$, where k_θ is the torsional stiffness, k_{66}, found in Table 5. Q for a cruciform hinge is given in Eq. (6). U is the total rib length (Norton [15]).

$$Q = \frac{U^2t^2}{3U + 1.8t} = \frac{w^2t^2}{3w + 1.8t} \qquad (6)$$

We finally arrive at Eq. (7) for a parametric range of motion equation:

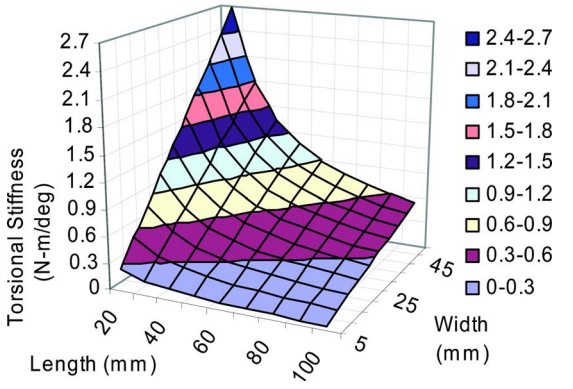

Fig. 18 *z*-rotational stiffness of CR joint (thickness=1 mm)

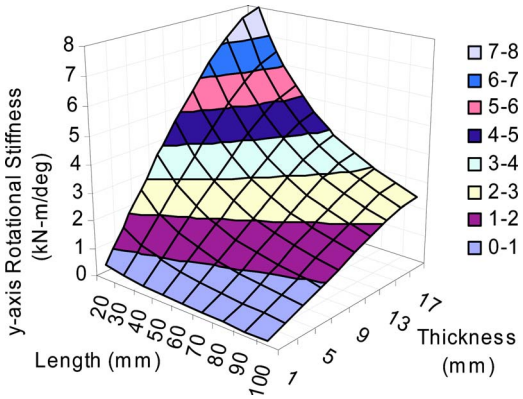

Fig. 19 *y*-bending/rotational stiffness of CR joint (width =20 mm)

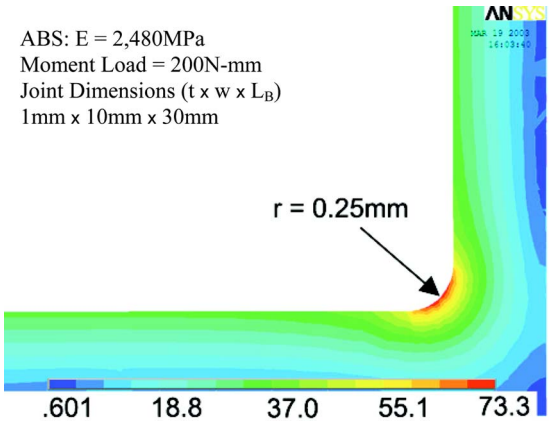

Fig. 21 Stress distribution about a fillet at an interior vertex (stress scale in MPa)

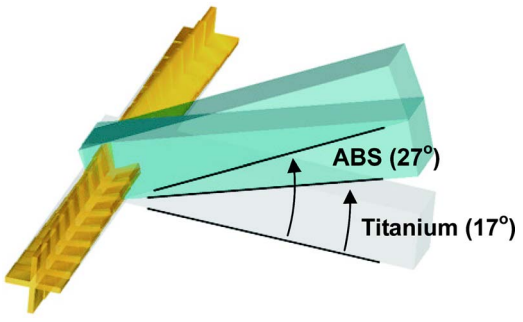

Fig. 22 Range of motion of CR joint

Table 7 Analytic vs numerical off-axis stiffness

Stiffness	Analytic	Numerical (ADAMS)	Analytic Error
Bending / Rotational (M_y/θ_y)	1,608,600 N-mm/rad	2,135,900 N-mm/rad	-25%
Bending (F_x/d_x)	3,016 N/mm	2,773 N/mm	+8.8%
Axial (F_z/d_z)	92,160 N/mm	92,202 N/mm	-0.05%

Table 8 Range of motion for 2 sample CR joints

	Titanium	ABS	units
Ansys R.O.M.	16.8	27.4	± deg.
Anal. R.O.M.	18.4 *(+9.5%)*	30.5 *(+11.3%)*	± deg.
M_z/θ_z	9900	207.6	N-mm/rad
M_y/θ_y	2,136,000	44,100	N-mm/rad
F_x/d_x	2,800	57.3	N/mm
F_z/d_z	92,200	1,900	N/mm
max load	3,200	128	N-mm
E	120,000	2,480	MPa
yield stress	1000	34.5	MPa

Table 9 Case 1: Equivalent longest length

	UM CR Joint		Split-Tube Joint		Free-Flex Joint (Cross-Pivot)		
torsional stiffness	207.6		246.4		26.5		N-mm
range of motion	27.4		62.1		159.4		deg.
dimensions	t	0.8	t	0.8	t	0.8	mm
	w	10	R	5	w	10	mm
	L	40	L	40	L	80	mm

$$\theta_{\max} = \frac{\tau_{\max} Q}{k_\theta} = \frac{\tau_{\max}}{2Gt} \frac{L}{\left(1 + 0.6\frac{t}{w}\right)\left(1 - 0.373\frac{t}{w}\right)} \tag{7}$$

Finite Element Range of Motion. Nonlinear finite element analysis is also performed to determine range of motion. Because initial analyses indicate a stress concentration on the internal edges between the cross arms, models with fillets along these edges (see Fig. 21) are also analyzed in an attempt to increase the range of motion.

Quadratic 10-noded tetrahedron elements are used for their torsional accuracy. Approximately 30,000 elements are required to resolve the stress concentrations and effects of end-constraints,

Table 10 Case 2: Equivalent volume

	UM CR Joint		Split-Tube Joint		Free-Flex Joint (Cross-Pivot)		
torsional stiffness	207.6		386.5		26.5		N-mm
range of motion	27.4		39.6		159.4		deg.
dimensions	t	0.8	t	0.8	t	0.8	mm
	w	10	R	5	w	10	mm
	L	40	L	25.5	L	80	mm

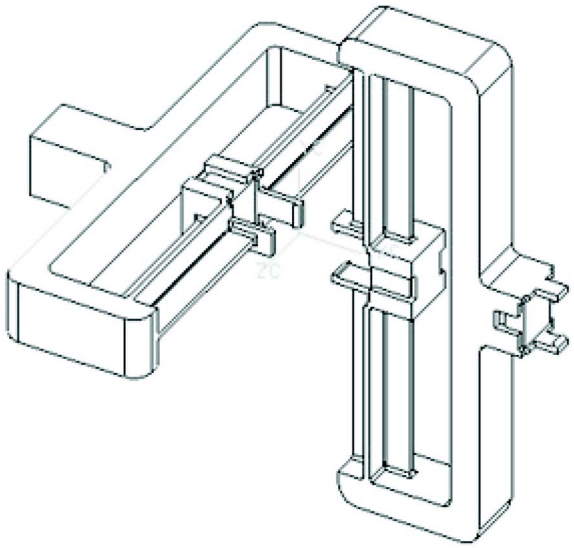

Fig. 23 Modular compliant revolute joints designed for plastic injection molding

with finer mesh resolution along the fillets and ends. Using fillet radii of 0.25 mm greatly reduces the stress concentrations, by more than 30%. A comparison of equally sized titanium and ABS plastic joints is given in Table 8. The parameters of the analyzed joint are the same as those used in Tables 6 and 7.

The analytic solutions consistently overestimate the FEA results, by 10%–15% for the above and other cases. The range of motion of the above-studied joints are shown in Fig. 22.

Joint Comparisons. Tables 9–12 provide quantitative comparisons of three revolute joints, looking at their torsional stiffness and range of motion. Four cases are provided, each using a different common characteristic: Longest length, material volume, range of motion, and torsional stiffness. Note that for the free-flex joint, L is the length of a single cross-beam; for the other joints, L is the length of one beam, i.e., one-half the total joint length. Also, "t" is beam thickness, "w" is beam width, and "R" is cylinder radius. Values in the tables are calculated from linear formulas and are for comparison. The larger range of motion values should be

Table 11 Case 3: Equivalent range of motion

	UM CR Joint		Split-Tube Joint		Free-Flex Joint (Cross-Pivot)		
torsional stiffness	207.6		874.9		472.6		N-mm
range of motion	27.4		27.3		27.2		deg.
dimensions	t	0.8	t	1	t	1.4	mm
	w	10	R	5	w	10	mm
	L	40	L	22	L	24	mm

Table 12 Case 4: Equivalent torsional stiffness

	UM CR Joint		Split-Tube Joint		Free-Flex Joint (Cross-Pivot)		
torsional stiffness	207.6		208.2		206.3		N-mm
range of motion	27.4		64.6		57.9		deg.
dimensions	t	0.8	t	0.75	t	1.1	mm
	w	10	R	5	w	15	mm
	L	40	L	39	L	40	mm

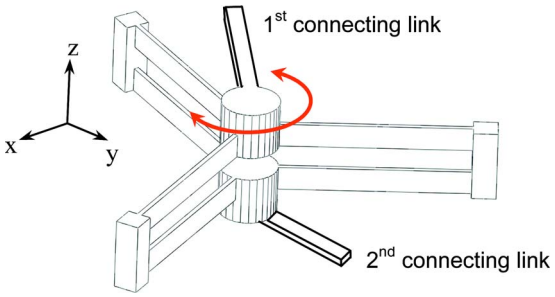

Fig. 24 Alternate CR joint conceptual design

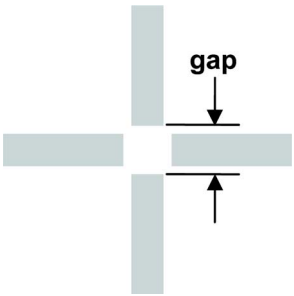

Fig. 27 Cross section of open-cross CR joint

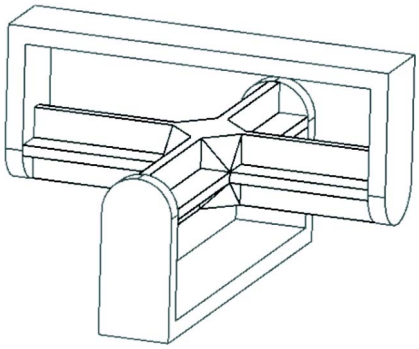

Fig. 25 CU joint conceptual design

verified with nonlinear numerical analysis.

All four cases show that the split-tube joint always has a greater range of motion than the CR joint, while the CR joint always has a better (lower) torsional stiffness. We also see that the free-flex joint often has both the best stiffness and the best range of motion. The free-flex joint, of course, has very large axis drift, but the designer should also question the definition of "compactness" at this point. The free-flex joint is effective at the cost of a large amount of space *in the plane of the mechanism*. The other two joints, however, take up negligible space in the mechanism plane; their longest dimensions are out-of-plane.

Manufacturability. The goal of fabrication from stock engineering parts has already been expressed. We have also designed the CR joint and Compliant Universal joint (see next section) to be fabricated via plastic injection molding. The joint can be made in components which snap-fit together to form either the CR or CU joint (see Fig. 23). With the fastening being rigid and occurring at noncompliant segments, these assembled joints should behave the same as the monolithic joints.

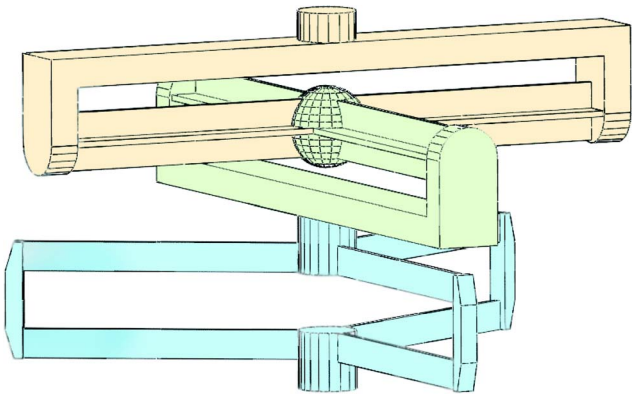

Fig. 26 CS joint conceptual design

Future Work

Other Compliant Joint Concepts. The CR joint in Fig. 13(*b*) requires a large space in the direction of the axis of rotation (motion axis). While this may be acceptable for some applications, others may be limited by different size constraints. An alternate CR joint configuration, shown in Fig. 24, allows for the tradeoff of joint footprint in the *xy*-plane and joint depth in the *z*-direction.

Compliant Universal Joint. To further increase the library of compliant joints for the design of generic mechanisms, two CR joints are concatenated to create a compliant universal (CU) joint (see Fig. 25).

The CU joint allows only two rotational degrees of freedom, as does its traditional mechanical counterpart. However, a compliant spherical (CS) joint with 3 degrees of freedom can be built by connecting CU and CR joints as demonstrated in Fig. 26.

Other work includes the integration of embedded sensors for deformation feedback, allowing for increased precision and repeatability in the micro- and nanometer range. Analysis on an "open-cross" CR joint (see Fig. 27) is also in progress. The elimination of the stress concentrations in the corners promises to allow for a much larger range of motion.

Conclusions

This paper presents new types of compliant joints for rotational and translational motions. The new compliant joint designs surpass the range of motion of many conventional flexure joints, while the combined achievements in off-axis stiffness ratio and zero axis drift make them very competitive with the latest advances in flexures. The joints presented in this paper are modeled and analyzed with analytical and CAE methods as appropriate. For a sample CR joint, the smallest and largest off-axis stiffnesses are 290 and 38,000 times the joint stiffness, respectively. Further, the overconstrained CT joint delivers exact straight-line motion and the CR joints have axis drift on the order of nanometers. The design charts presented in this paper, based on extensive parametric analyses, aid in sizing the joints for various applications.

Acknowledgments

The authors gratefully acknowledge the financial support of the NSF Engineering Research Center for Reconfigurable Machining Systems (NSF Grant No. EEC95-92125) at the University of Michigan and the valuable input from the Center's industrial partners. Brian Trease is further supported by a National Science Foundation Graduate Research Fellowship.

References

[1] Paros, J. M., and Weisbord, L., 1965, "How to Design Flexure Hinges," Mach. Des., **37**(27), pp. 151–156.
[2] Pernette, E., Henein, S., Magnani, I., and Clavel, R., 1997, "Design of Parallel Robots in Microrobotics," Robotica, **15**, pp. 417–420.
[3] Howell, L. L., 2001, *Compliant Mechanisms*, Wiley, New York.
[4] Lobontiu, N., Paine, J., Garcia, E., and Goldfarb, M., 2001, "Corner-Filleted Flexure Hinges," ASME J. Mech. Des., **123**(3), pp. 346–352.
[5] Lobontiu, N., and Paine, J., 2002, "Design of Circular Cross-Section Corner-

Filleted Flexure Hinges for Three-Dimensional Compliant Mechanisms," ASME J. Mech. Des., **124**(3), pp. 479–484.
[6] Carricato, M., Parenti-Castelli, V., and Duffy, J., 2001, "Inverse Static Analysis of a Planar System With Flexural Pivots," ASME J. Mech. Des., **123**(1), pp. 43–50.
[7] Smith, S., 2000, *Flexures, Elements of Elastic Mechanisms*, Taylor & Francis, London, England.
[8] Saggere, L., Kota, S., and Crary, S. B., 1994, "A New Design for Suspension of Linear Microactuators," Proceedings, DSC-Vol 55-2, Dynamic Systems and Control, Vol. 2, 1994 International Mechanical Engineering Congress and Exposition, Chicago, IL, Nov. 6–11, pp. 671–675.
[9] Lobontiu, N., 2002, *Compliant Mechanisms: Design of Flexure Hinges*, CRC Press, Boca Raton, FL.
[10] Kyusojin, A., and Sagawa, D., 1988, "Development of Linear and Rotary Movement Mechanism by Using Flexible Strips," Bull. Jpn. Soc. Precis. Eng., **22**(4), pp. 309–314.
[11] Bona, F., and Zelenika, S., 1994, "Precision Positioning Devices Based on Elastic Elements: Mathematical Modeling and Interferometric Characterization," Seminar on Handling and Assembly of Microparts, Vienna, Austria.
[12] Weinstein, W., 1965, "Flexure-Pivot Bearings," Mach. Des., **37**(13-D), pp. 150–157.
[13] Goldfarb, M., and Speich, J., 1999, "A Well-Behaved Revolute Flexure Joint for Compliant Mechanism Design," ASME J. Mech. Des., **121**(3), pp. 424–429.
[14] Haringx, J. A., 1949, "The Cross Spring Pivot as a Constructional Element," Appl. Sci. Res., Sect. A, **A1**(5–6), pp. 313–332.
[15] Norton, R., 2000, *Machine Design, An Integrated Approach*, 2nd ed., Prentice Hall, Upper Saddle River, NJ.